Author's personal copy

Available online at www.sciencedirect.com

SciVerse ScienceDirect

Geochimica et Cosmochimica Acta 107 (2013) 12–26

Geochimica et Cosmochimica Acta

www.elsevier.com/locate/gca

Iron isotopic systematics of oceanic basalts

Fang-Zhen Teng [a,b,*], Nicolas Dauphas [b], Shichun Huang [c], Bernard Marty [d]

[a] Isotope Laboratory, Department of Geosciences and Arkansas Center for Space and Planetary Sciences, University of Arkansas, 113 Ozark Hall, Fayetteville, AR 72701, USA

[b] Origins Laboratory, Department of the Geophysical Sciences and Enrico Fermi Institute, The University of Chicago, 5734 South Ellis Avenue, Chicago, IL 60637, USA

[c] Department of Earth and Planetary Sciences, Harvard University, 20 Oxford Street, Cambridge, MA 02138, USA

[d] Centre de Recherches Pétrographiques et Géochimiques, CNRS, 15 Rue Notre-Dame-des-Pauvres, 54501 Vandoeuvre-lès-Nancy, France

Received 10 June 2012; accepted in revised form 24 December 2012; Available online 4 January 2013

Abstract

The iron isotopic compositions of 93 well-characterized basalts from geochemically and geologically diverse mid-ocean ridge segments, oceanic islands and back arc basins were measured. Forty-three MORBs have homogeneous Fe isotopic composition, with δ^{56}Fe ranging from +0.07‰ to +0.14‰ and an average of $+0.105 \pm 0.006$‰ ($2SD/\sqrt{n}$, $n = 43$, MSWD = 1.9). Three back arc basin basalts have similar δ^{56}Fe to MORBs. By contrast, OIBs are slightly heterogeneous with δ^{56}Fe ranging from +0.05‰ to +0.14‰ in samples from Koolau and Loihi, Hawaii, and from +0.09‰ to +0.18‰ in samples from the Society Islands and Cook-Austral chain, French Polynesia. Overall, oceanic basalts are isotopically heavier than mantle peridotite and pyroxenite xenoliths, reflecting Fe isotope fractionation during partial melting of the mantle. Iron isotopic variations in OIBs mainly reflect Fe isotope fractionation during fractional crystallization of olivine and pyroxene, enhanced by source heterogeneity in Koolau samples.

© 2012 Elsevier Ltd. All rights reserved.

1. INTRODUCTION

The magnitude of equilibrium isotope fractionation decreases with increasing temperature and atomic mass, and is likely to be small for isotopes of heavy elements during high-temperature processes (Bigeleisen and Mayer, 1947; Urey, 1947). On the other hand, isotope fractionation associated with kinetic processes such as chemical diffusion, Soret effect, or evaporation/condensation can remain significant at high temperatures (Richter et al., 2009). Recent high-precision isotopic analyses of natural samples have shown that measurable Fe isotope fractionation could occur at both whole-rock (>0.2‰) and mineral scales (>1.6‰) during mantle melting (Williams et al., 2004, 2005, 2009; Weyer et al., 2005; Weyer and Ionov, 2007; Dauphas et al., 2009a; Zhao et al., 2010, 2012; Huang et al., 2011c; Hibbert et al., 2012) and igneous differentiation (Poitrasson and Freydier, 2005; Heimann et al., 2008; Teng et al., 2008, 2011; Schoenberg et al., 2009; Schuessler et al., 2009; Weyer and Seitz, 2012; Telus et al., 2012). The fractionation of Fe isotopes at high temperatures could be produced by kinetic or equilibrium processes and may be associated with changes in the oxidation state of Fe.

Studying the mechanism associated with high-temperature Fe isotope fractionation is important to further our understanding of the theory on stable isotope fractionation and to use Fe isotopes as tracers of petrogenetic processes. For example, compared to chondrites (Poitrasson et al., 2005; Schoenberg and von Blanckenburg, 2006; Dauphas et al., 2009a; Craddock and Dauphas, 2010), terrestrial and lunar basalts have heavy Fe isotopic compositions (Beard et al., 2003; Poitrasson et al., 2004; Schoenberg and von Blanckenburg, 2006; Weyer and Ionov, 2007; Teng et al., 2008; Schuessler et al., 2009; Dauphas et al., 2009a;

* Corresponding author. Present address: Department of Earth and Space Sciences, University of Washington, Johnson Hall Rm-070, Box 351310, 4000 15th Avenue NE, Seattle, WA 98195, USA.
E-mail address: fteng@uw.edu (F.-Z. Teng).

0016-7037/$ - see front matter © 2012 Elsevier Ltd. All rights reserved.
http://dx.doi.org/10.1016/j.gca.2012.12.027

Author's personal copy

Craddock et al., 2010; Liu et al., 2010), which was initially ascribed to evaporation-driven kinetic Fe isotope fractionation during the giant impact that formed the Moon, resulting in a non-chondritic Fe isotopic composition of terrestrial and lunar mantles (Poitrasson et al., 2004). Polyakov (2009) and Williams et al. (2012) proposed instead that this reflected high-pressure equilibrium Fe isotope fractionation between metal and silicate during core formation or disproportionation of Fe^{2+} into Fe^{0} and Fe^{3+}, which produced a non-chondritic mantle that was later sampled by terrestrial basalts. Alternatively, the difference in Fe isotopic composition between basalts and chondrites may result from Fe isotope fractionation during partial melting of the mantle (Weyer and Ionov, 2007; Dauphas et al., 2009a).

Additional complications arise from the fact that Fe isotopes can also be fractionated during fractional crystallization of magma (Teng et al., 2008, 2011; Schuessler et al., 2009; Weyer and Seitz 2012). Consequently, basalts are not representative of their mantle sources. Indeed, global mantle xenoliths and high-degree partial melts have, on average, a Fe isotopic composition more similar to chondrites, suggesting a chondritic Fe isotopic composition of the Earth (Williams et al., 2004, 2005; Weyer et al., 2005; Weyer and Ionov, 2007; Dauphas et al., 2009a, 2010; Zhao et al., 2010, 2012; Huang et al., 2011c; Hibbert et al., 2012; Craddock et al., 2013). Accordingly, complex models that invoke evaporation-induced kinetic isotope fractionation during moon-forming giant impact (Poitrasson et al., 2004) or equilibrium Fe isotope fractionation during core formation or Fe disproportionation (Polyakov, 2009; Williams et al., 2012) may not be needed.

In order to further constrain the extent to which partial melting and magmatic differentiation affect the Fe isotopic compositions of igneous rocks, mid-ocean ridge basalts (MORBs), ocean island basalts (OIBs) and back arc basin basalts (BABBs) were analyzed. The results show that MORBs and BABBs have homogeneous Fe isotopic composition whereas OIBs are isotopically heterogeneous. On average, MORBs, BABBs and OIBs are isotopically heavier than average mantle xenoliths, reflecting Fe isotope fractionation during partial melting of the mantle and magma differentiation.

2. SAMPLES

Except for a few studies (Weyer and Ionov, 2007; Teng et al., 2008; Schuessler et al., 2009), most previously investigated oceanic basalts focused on geostandards (Poitrasson et al., 2004; Weyer et al., 2005; Williams et al., 2005; Schoenberg and von Blanckenburg, 2006; Dauphas et al., 2009a,b; Craddock and Dauphas, 2010). Here, a geographically dispersed, chemically diverse set of well-characterized samples, including 43 MORBs covering major ridge segments, 47 OIBs from Hawaiian and French Polynesian islands, and 3 BABBs from North Fiji basin have been investigated (Fig. 1). To avoid the effect of alteration on Fe isotopes (Rouxel et al., 2003), all samples chosen here are fresh, as evidenced by their chemical compositions, their appearance under a binocular microscope, and studies of nitrogen isotopes and noble gases that are extremely sensitive to seawater alteration (Marty and Humbert, 1997; Marty and Tolstikhin, 1998; Marty and Zimmermann, 1999; Marty and Dauphas, 2003). Major- and trace-element abundances and radiogenic and stable isotopic data for these samples have been reported elsewhere (Devey et al., 1990; Chauvel et al., 1992; Woodhead et al., 1993; Frey et al., 1994; Marty and Humbert, 1997; Lassiter and Hauri, 1998; Marty and Tolstikhin, 1998; Marty and Zimmermann, 1999; Marty and Dauphas, 2003; Huang and Frey, 2005; Teng et al., 2010). A brief description of these samples is given below.

2.1. MORBs (n = 43) and BABBs (n = 3)

Large variations of chemical and isotopic compositions in all major ocean basins indicate that the different regions of the upper mantle have not been effectively mixed (BVSP, 1981; Hofmann, 2003). Based on chemical compositions, MORBs can be divided into three types: N-MORB (normal), E-MORB (enriched) and T-MORB (transitional). N-MORBs have $K_2O < 0.1$, $(La/Sm)_{CI} < 1.0$ and $TiO_2 < 1.0$, whereas E-MORBs have $K_2O > 0.1$, $(La/Sm)_{CI} > 1.7$ and $TiO_2 > 1.0$, for the same Mg#. T-MORBs have intermediate values.

MORB glasses investigated here are quenched submarine magmas from zero-age centered ridge sections including the Mid-Atlantic Ridge at 24–36°N, the East Pacific Rise at 13°N, 06°N, 17–19°S, and 21°N, the Indian Ridge system near the Rodriguez Triple Junction and at 39°S, and the Red Sea at 18°N and 20°N (Table 1). In addition, samples from the North Fiji Basin, the world's largest back arc basin, have also been analyzed (Table 1). All these MORB and BABB samples are fresh basaltic lavas, with the usual morphologies of submarine tubes or pillow lavas rimmed by glassy crusts about 1.5 cm thick. They cover several major mid-oceanic ridge segments, are well-characterized and span a broad range in chemical and radiogenic isotope compositions. These basalts vary from N-MORB, T-MORB to E-MORB. Their chemical compositions range from 6.4 to 9.7 wt.% in MgO, from 0.03 to 0.31 wt.% in K_2O, from 0.76 to 2.27 wt.% in TiO_2 and from 0.02 to 0.21 in K_2O/TiO_2 ratios (Table 1, Fig. 2). The spreading rates of ridge segments vary from 1 to 2 cm/year at the Mid-Atlantic Ridge to 8–9 cm/year at the East Pacific Rise (Marty and Humbert, 1997; Marty and Tolstikhin, 1998; Marty and Zimmermann, 1999). The Mg isotopic compositions of these MORBs were previously reported in Teng et al. (2010).

2.2. OIBs and related samples (n = 47)

OIBs sample the deep mantle and are chemically and isotopically more variable than MORBs, which has been interpreted to result from crustal recycling, core-mantle interactions, and a different history of melt extraction (Hofmann, 2003). In detail, isotopic (e.g., Sr, Nd, Pb) heterogeneity in the mantle can be accounted for by mixing of at least five mantle end-members (i.e., HIMU, EM-1, EM-2, FOZO and DMM, Zindler and Hart, 1986; Hart et al.,

Author's personal copy

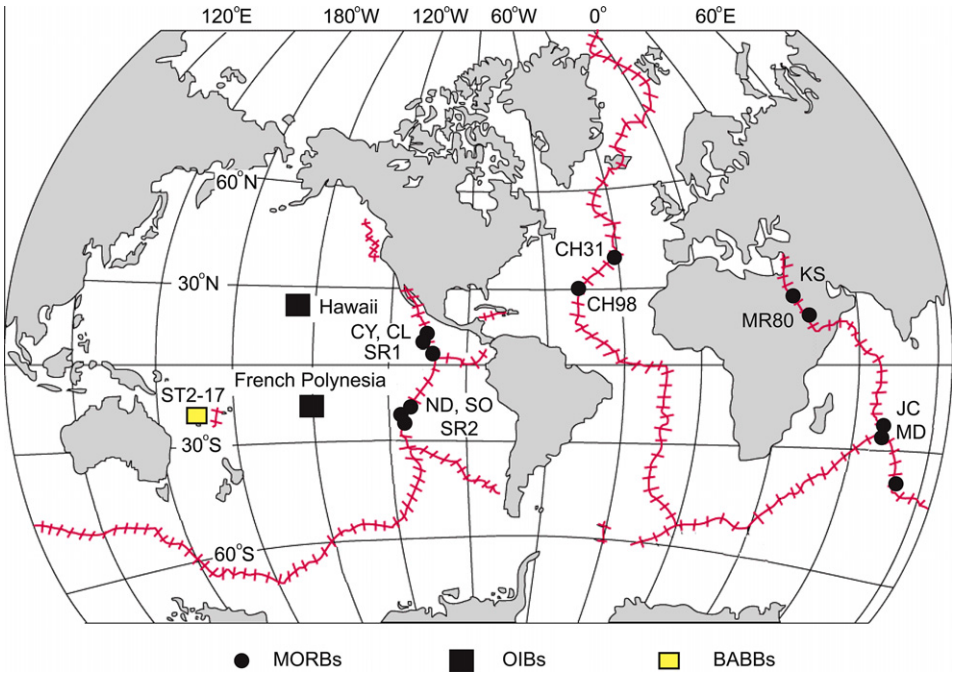

Fig. 1. Sample location map for mid-ocean ridge basalts (MORBs), ocean island basalts (OIBs) and back arc basin basalts (BABBs) investigated in this study. Modified from Teng et al. (2010).

1992). Further examination of global datasets shows that OIBs derived from different mantle end-members as defined by studies of radiogenic isotopes also have distinct major element characteristics (Hauri, 1996; Jackson and Dasgupta, 2008). The OIB samples selected for this study are lavas from two well-studied islands in the Pacific Ocean with a large range in compositions: Hawaii (Makapuu-stage of Koolau and Loihi) and French Polynesia (Society Islands and Cook-Austral chain) (Figs. 1 and 3).

The Hawaiian Islands are the best studied of all the ocean islands. Samples investigated here are from Koolau volcano and Loihi seamount (Table 2). Together with lavas from Kilauea volcano (Teng et al., 2008), these samples cover the major end-members found in Hawaiian lavas (e.g., Jackson et al., 2012). The Makapuu-stage Koolau lavas define one of the most extreme isotopic compositional endmembers among Hawaiian shield-stage lavas and their petrogenesis may involve melting of eclogites formed by recycling of oceanic crust (Hauri, 1996; Lassiter and Hauri, 1998; Norman and Garcia, 1999; Huang and Frey, 2005; Sobolev et al., 2005, 2007; Huang et al., 2007, 2011a). Of them, KOO17A investigated in Teng et al. (2011) and KOO17 studied here were collected from the same lava flow but KOO17A is more olivine-rich as evidenced by the high modal abundance of olivine and by its high bulk MgO content (21.5 wt.%) (Frey et al., 1994). In addition, four samples from Loihi Seamount were also investigated (Valbracht et al., 1996). The Loihi basalts studied here are mainly alkaline and have been previously investigated for Fe isotopes, albeit with low precision (Dauphas et al., 2004). Magnesium isotopic compositions of these Hawaiian samples were previously reported in Teng et al. (2010).

The Polynesian islands are located in the South Pacific Ocean and consist of six main archipelagos (Society, Marquesas, Tuamotu, Gambier and Cook-Austral chain). Lavas of Polynesian islands are alkaline and are derived from three of the main geochemical mantle end-members: HIMU, EM1 and EM2 (Zindler and Hart, 1986) although their mantle source dynamics are still debated (e.g., Vidal et al., 1984; McNutt and Fischer, 1987; Hekinian et al., 1991; Chauvel et al., 1992, 2012; Huang et al., 2011b). The 23 samples investigated here are from the Society Islands (Teahitia, Mehetia, Cyana, Rocard and small nearby seamounts) and Cook-Austral (MacDonald) chain (Table 2). They are mainly basaltic glasses with five evolved samples having low MgO (0.68–1.19 wt.%) and high SiO_2 (59.9–61.0 wt.%) contents, which are thought to result from the removal of up to 70% cumulate from basalts (Hekinian et al., 1991). These 23 samples are enriched in incompatible trace elements, radiogenic isotopes and ^{18}O, and are highly variable in N isotopic compositions. These geochemical and isotopic features are consistent with derivation from a long-term enriched source that mixed up to 9% recycled crust containing a substantial proportion of pelagic sediments (Devey et al., 1990; Chauvel et al., 1992; Woodhead et al., 1993; Eiler et al., 1997; Dauphas and Marty, 1999; Marty and Dauphas, 2003). The Mg isotopic compositions of these samples were previously reported in Teng et al. (2010).

3. ANALYTICAL METHODS

Iron isotopic analyses were carried out at the Origins Laboratory of the University of Chicago. The detailed protocols for sample dissolution, column chemistry and

Author's personal copy

Table 1
Iron isotopic compositions of mid-ocean ridge basalts and back arc basin basalts.

Sample	Type	MgO (wt.%)	K_2O/TiO_2	$Na_{8.0}$	*n*	$\delta^{56}Fe$	95% c.i.	$\delta^{57}Fe$	95% c.i.
Mid Atlantic Ridge									
CH31DR01	E	8.97	0.15	2.67	9	0.074	0.034	0.113	0.057
CH31DR02	E	7.93	0.13	2.26	9	0.124	0.034	0.174	0.057
CH31 DR11	E	8.36	0.16	2.47	9	0.143	0.026	0.221	0.039
CH31 DR12	E	7.7	0.06	1.74	9	0.123	0.034	0.176	0.057
CH98 DR08	N				9	0.118	0.034	0.188	0.057
CH98 DR12	N	7.69	0.03	2.57	9	0.127	0.034	0.195	0.057
CH98 DR15	N	8.43	0.06	2.61	9	0.101	0.034	0.159	0.057
CH98 DR17	N	7.77	0.07	2.81	9	0.139	0.026	0.175	0.033
East Pacific Rise									
CL DR01	N	8.15	0.06	2.73	9	0.096	0.026	0.128	0.033
CY82-21-06	T	8.04	0.11	2.26	9	0.117	0.031	0.154	0.033
CY82-31-02V	N	8.52	0.06	2.67	9	0.095	0.026	0.130	0.033
CY82-31-01	N	8.97	0.04	3.00	9	0.130	0.026	0.177	0.033
CY84-05-08	N	7.21	0.03	2.68	9	0.126	0.026	0.202	0.033
SR1 DR04	N	6.99	0.04	2.58	9	0.087	0.028	0.122	0.038
SO40 G136D	N	7.64	0.04	2.56	9	0.106	0.028	0.160	0.045
SO40 G178D	N	7.92	0.06	2.89	9	0.128	0.026	0.151	0.047
SO40 G154D	N	7.89	0.04	2.69	9	0.087	0.026	0.139	0.047
SO40 G193h	N	7.3	0.08	2.84	5	0.079	0.029	0.126	0.046
SO26 G184D	N	7.03	0.05	2.62	9	0.101	0.028	0.179	0.045
SO62 G324G	N	6.41	0.06	2.30	5	0.101	0.029	0.158	0.046
SO62 G296G	N	7.88	0.06	2.47	3	0.084	0.046	0.118	0.051
SO62 G287G	N	7.92	0.07	2.52	3	0.099	0.046	0.149	0.051
SR2 DR02	N	7.33	0.02	2.74	9	0.104	0.028	0.144	0.038
SR2 DR03	N	7.3	0.02	2.64	9	0.106	0.028	0.146	0.038
SR2 DR-7	N				4	0.106	0.027	0.145	0.038
ND12-2	N	7.51	0.03	2.85	9	0.133	0.026	0.202	0.034
ND15-4	N	7.31	0.03	2.67	9	0.110	0.026	0.141	0.034
ND18-1	T	6.9	0.11	2.64	9	0.128	0.026	0.179	0.034
ND21-3	N	7.36	0.03	2.72	9	0.076	0.026	0.143	0.034
ND21-4	N	8.04	0.04	2.70	9	0.080	0.028	0.109	0.038
Indian Ocean									
HY09-07	N	8.09	0.04	2.85	9	0.098	0.026	0.129	0.033
JC 030703 D1	N	7.86	0.07	2.90	9	0.107	0.026	0.156	0.034
JC 217 D1	N	7.53	0.05	2.77	9	0.095	0.026	0.133	0.034
MD57 D4-4	N	8.53	0.04	2.45	9	0.077	0.027	0.107	0.039
MD57 D9-9	N	9.73	0.08	2.81	5	0.101	0.032	0.155	0.054
MD22-3	N				5	0.088	0.032	0.129	0.054
MD23-1	N	7.38	0.06	2.53	5	0.125	0.032	0.167	0.054
MD23-2	T				5	0.088	0.032	0.111	0.054
MD23 site-2	T	8.53	0.10	2.94	5	0.080	0.032	0.126	0.054
MD23 site 4	T	8.63	0.09	3.80	5	0.141	0.032	0.201	0.054
Red Sea									
KS11A	E	6.9	0.21	2.68	9	0.102	0.026	0.153	0.034
MR80 57-1	T	7.9	0.10	1.68	5	0.117	0.032	0.120	0.054
MR80 59-2	T	8.4	0.07	1.97	5	0.073	0.032	0.066	0.054
North Fiji Basin (BABBs)[a]									
ST2-17-6	T	7.46	0.13	2.48	9	0.106	0.028	0.155	0.038
ST2-17-7	N	7.31	0.03	2.37	9	0.087	0.028	0.131	0.038
ST2-17-10	T	7.4	0.12	2.45	9	0.095	0.028	0.139	0.038

$^{x}Fe = [(^{x}Fe/^{54}Fe)_{sample}/(^{x}Fe/^{54}Fe)_{IRMM\text{-}014} - 1] \times 1000$, where $x = 56$ or 57; 95% c.i. stands for 95% confidence interval of the mean for n replicate analyses of the same solution and it integrates the long-term reproducibility based on replicate analyses of BHVO-1 standard (Dauphas et al., 2009b). MgO and K_2O/TiO_2 data are from Marty and Zimmermann (1999).

[a] BABBs mean back arc basin basalts. See text for references on sample locations.

isotopic analyses have been reported in Dauphas et al. (2009b) and Craddock and Dauphas (2010). Only a brief description is given below.

Fresh basalt samples, usually 1–5 mg glass fragments, were crushed in an agate mortar, cleaned with Milli-Q water for 10 min, three times, in an ultrasonic bath before

Author's personal copy

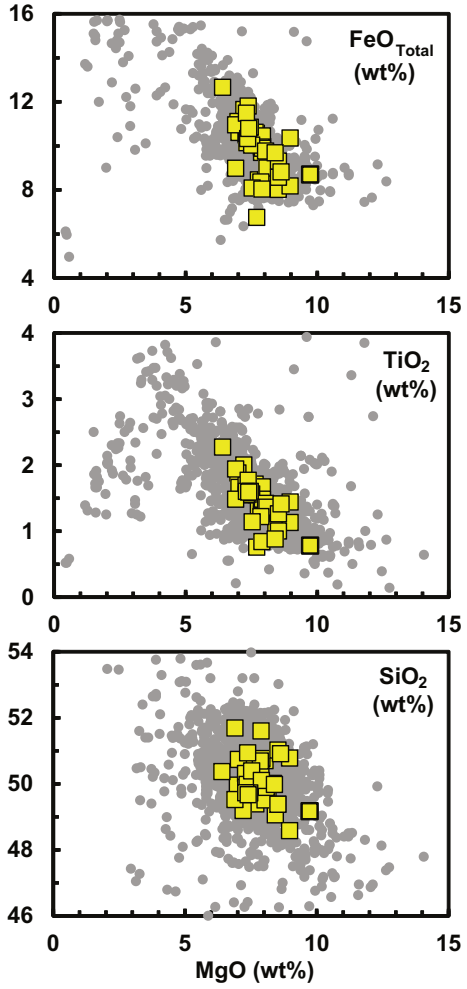

Fig. 2. TiO_2, SiO_2 and FeO_{Total} vs. MgO in MORB samples investigated in this study (yellow squares). Grey dots represent MORBs using global literature dataset (PetDB: http://www.earthchem.org/petdb). (For interpretation of the references to colour in this figure legend, the reader is referred to the web version of this article.)

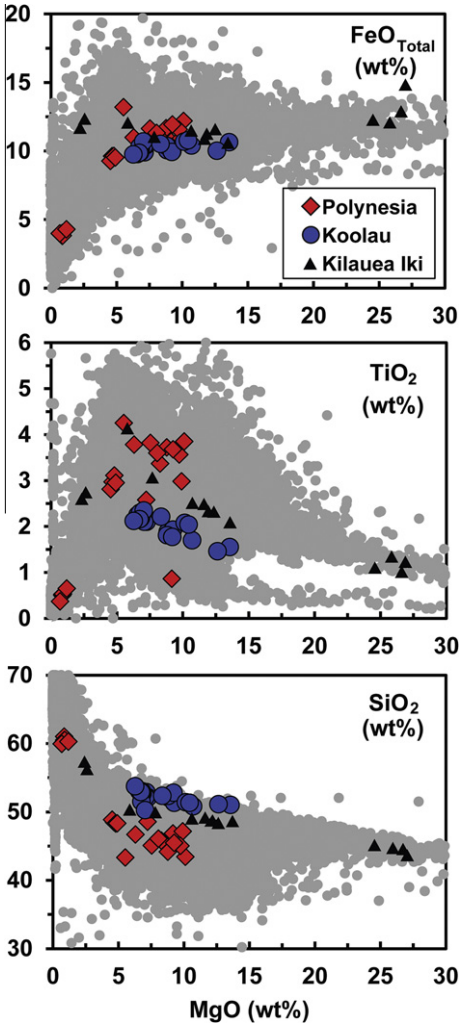

Fig. 3. TiO_2, SiO_2 and FeO_{Total} vs. MgO in OIB samples investigated in this study. In this and subsequent plots, "Polynesia" represents samples from the Society Islands and Cook-Austral chain. "Koolau" represents samples from Koolau, Hawaii. Kilauea Iki lavas are also plotted for comparison (Helz 1987; Helz et al., 1994; Teng et al., 2008). Samples from Loihi are not plotted due to the lack of MgO contents. Grey dots represent OIB using global literature dataset (GEOROC: http://georoc.mpch-mainz.gwdg.de/georoc/).

dissolution. All samples were dissolved in a combination of concentrated HF–$HClO_4$–HNO_3. Iron was purified on an anion exchange resin (Bio-Rad AG1-X8, 200–400 mesh) in HCl medium. Purified Fe sample solutions were introduced into the Ar plasma using a Thermo Scientific quartz cyclonic spray chamber fitted with a 100 μL/min microneb-ulizer from Elemental Scientific Inc. Samples were analyzed using a Neptune MC-ICPMS, with ^{53}Cr, ^{54}Fe, ^{56}Fe, ^{57}Fe, ^{58}Fe and ^{60}Ni ion beams measured simultaneously on Far-aday cups at medium resolution. Each sample analysis is bracketed by measurements of the IRMM-014 standard, a reference material that is made of pure Fe metal (Taylor et al., 1992) and has an isotopic composition that is indis-tinguishable from chondritic value (Craddock and Dauphas 2010). Iron isotope data are reported in standard δ-notation in per mil relative to IRMM-014: $\delta^i Fe = [(^iFe/^{54}Fe)_{sample}/(^i\text{-}Fe/^{54}Fe)_{IRMM\text{-}014} - 1] \times 1000$, where i refers to 56 or 57. The concentrations of the samples and bracketing stan-dards (1–2 ppm) were matched to within ±10%. With an uptake rate of 100 μL/min, a 1 ppm solution typically pro-duces 6–10 V ^{56}Fe signal at medium resolution and 1–2 V ^{56}Fe signal at high resolution (with a 10^{11} Ω resistor for the Faraday cups). The precision on $^{56}Fe/^{54}Fe$ ratio, with n repeat runs (typically $n = 9$, with less repeats if high pre-cision is achieved) of one block of 25 cycles of 8 s each, is <0.04‰ (95% confidence interval). The quoted uncertainty encompasses within-session as well as long-term external reproducibility (Dauphas et al., 2009b).

4. RESULTS

Iron isotopic compositions are reported in Table 1 for MORBs and BABBs, Table 2 for OIBs and are summarized

Author's personal copy

Table 2
Iron isotopic compositions of ocean island basalts.

Sample	MgO (wt.%)	CaO (wt.%)	*N*	δ^{56}Fe	95% c.i.	δ^{57}Fe	95% c.i.
Society Islands and Cook-Austral chain, French Polynesia							
Seamount No.1, Society							
DTH 02-01	0.86	1.32	9	0.131	0.028	0.164	0.045
DTH 02-02	0.86	1.33	3	0.115	0.046	0.152	0.051
Seamount No.2, Society							
DTH 03-03	9.16	10.58	3	0.106	0.046	0.125	0.051
Seamount No.3, Society							
DTH 04-01	0.91	1.41	9	0.134	0.028	0.173	0.045
DTH 04-04			3	0.157	0.046	0.162	0.051
Seamount No.4, Society							
DTH 05-02	0.68	1.25	9	0.142	0.028	0.187	0.045
Teahitia, Society							
SO47 37GC			5	0.091	0.029	0.118	0.046
TH09-02	10.11	11.89	9	0.135	0.027	0.212	0.039
TH09-05	8.78	11.54	9	0.141	0.027	0.231	0.039
SO47-9DS	9.91	8.80	5	0.156	0.029	0.230	0.046
SO47 5DS-1	8.28	8.70	5	0.117	0.037	0.166	0.049
TH11-01	7.54	11.83	6	0.146	0.031	0.234	0.048
TH12-01	9.74	11.28	9	0.152	0.031	0.152	0.048
TH12-06	4.67	7.15	9	0.181	0.026	0.252	0.039
TH14-02	4.53	7.01	9	0.174	0.026	0.259	0.039
TH14-03	4.8	7.36	9	0.182	0.026	0.269	0.047
TH14-05	4.91	7.12	9	0.161	0.026	0.247	0.039
Mehetia, Society							
TH10-04	9.26	9.89	9	0.138	0.027	0.210	0.039
Rocard, Society							
TH21	6.31	9.98	9	0.151	0.026	0.244	0.047
SO47 34DS-1	8.06	9.44	5	0.149	0.029	0.239	0.046
Cyana, Society							
TH25-03	1.19	1.44	9	0.117	0.026	0.113	0.047
MacDonald, Cook-Austral							
TH28-07	7.23	11.48	9	0.125	0.026	0.134	0.047
TH30-03	5.53	12.03	9	0.133	0.026	0.199	0.039
Koolau, Hawaii							
KOO1	7.14	9.46	9	0.104	0.030	0.134	0.048
Replicate			9	0.112	0.034	0.130	0.061
KOO7	6.99	9.90	9	0.136	0.030	0.187	0.048
Replicate			9	0.144	0.034	0.190	0.061
KOO8	7.25	9.79	9	0.065	0.030	0.105	0.048
KOO15	7.08	8.93	9	0.104	0.034	0.136	0.048
KOO17	8.86	8.78	9	0.080	0.030	0.141	0.048
KOO17A[a]	21.54	5.82	9	−0.011	0.030	−0.017	0.040
KOO19	6.58	9.24	9	0.100	0.030	0.160	0.048
Replicate			9	0.098	0.034	0.163	0.061
KOO21	9.26	8.60	9	0.089	0.030	0.128	0.048
Replicate			9	0.096	0.034	0.143	0.061
KOO24	8.81	8.78	9	0.082	0.030	0.131	0.047
Replicate			9	0.081	0.033	0.130	0.043
KOO32	9.21	8.54	9	0.092	0.029	0.142	0.038
KOO48	6.84	9.72	9	0.120	0.029	0.135	0.038
KOO49	10.15	8.71	9	0.100	0.029	0.148	0.038
Replicate			9	0.0941	0.033	0.142	0.047
KOO55	8.35	8.98	9	0.096	0.029	0.142	0.038
KOO-55D	10.44	8.30	9	0.076	0.029	0.127	0.038
KM-1	13.57	7.55	9	0.079	0.033	0.118	0.043
KM-3	12.64	8.04	9	0.105	0.030	0.118	0.039

Author's personal copy

Table 2
(*continued*)

Sample	MgO (wt.%)	CaO (wt.%)	*N*	δ^{56}Fe	95% c.i.	δ^{57}Fe	95% c.i.
OH-21	6.83	9.10	9	0.115	0.029	0.169	0.038
OH-22	6.76	9.43	9	0.101	0.031	0.135	0.047
Replicate			9	0.095	0.029	0.158	0.050
OH-24	6.79	9.11	9	0.119	0.029	0.151	0.038
OH-26	6.72	9.09	9	0.083	0.025	0.131	0.040
OH-27	6.28	9.07	9	0.100	0.031	0.118	0.039
Loihi, Hawaii							
T4D2#1			6	0.047	0.029	0.073	0.047
Replicate			6	0.076	0.029	0.088	0.038
T4D4-01			6	0.094	0.029	0.138	0.048
T4D3#3			6	0.067	0.029	0.099	0.047
T4D3#7			6	0.056	0.029	0.118	0.047

$\delta^x Fe = [(^xFe/^{54}Fe)_{sample}/(^xFe/^{54}Fe)_{IRMM\text{-}014} - 1] \times 1000$, where $x = 56$ or 57; 95% c.i. stands for 95% confidence interval of the mean for *n* replicate analyses of the same solution and it integrates the long-term reproducibility based on replicate analyses of BHVO-1 standard (Dauphas et al., 2009b). Replicate: repeat column chemistry from the same stock sample solution analyzed by the sample-standard bracketing method. MgO and CaO data are from Norman and Garcia (1999), Frey et al. (1994) and this study.

[a] Data are from Teng et al. (2011). See text for references on sample locations.

as histograms in Fig. 4 for all oceanic basalts as well as literature oceanic basalt data.

4.1. Iron isotopic compositions of BABBs and MORBs

Iron isotopic compositions of the 43 MORBs, including N-, E- and T-types from different locations and with different radiogenic and stable isotopic ratios, are homogeneous, with δ^{56}Fe values ranging from +0.07 to +0.14‰ with an average of $+0.105 \pm 0.006$‰ ($2SD/\sqrt{n}$, $n = 43$) (Fig. 4). δ^{56}Fe values vary from +0.07 to +0.14‰ in Mid Atlantic MORBs ($n = 8$), from +0.08 to +0.13‰ in East Pacific Rise MORBs ($n = 22$), from +0.08 to +0.14‰ in Indian MORBs ($n = 10$), from +0.07 to +0.12‰ in Red Sea basalts ($n = 3$) and from +0.09 to +0.11‰ in North Fiji BABBs ($n = 3$). These values agree with the few high-precision Fe isotopic data of MORBs published thus far ($n = 8$; Weyer and Ionov, 2007; Teng et al., 2008). To the best of our knowledge, the three North Fiji lavas are the first published Fe isotopic data for BABBs.

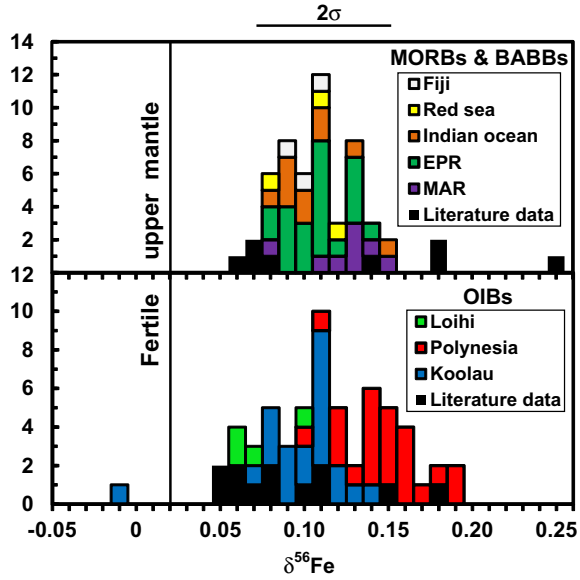

Fig. 4. Iron isotopic compositions of MORBs, OIBs and BABBs investigated in this study. Data are reported in Tables 1 and 2. Literature oceanic basalt data are from Weyer and Ionov (2007), Teng et al. (2008) and Schuessler et al. (2009). Geostandards BHVO-1 and BIR-1 data are from Craddock and Dauphas (2010). The grey vertical solid line represents the Fe isotopic composition of the fertile upper mantle ($\delta^{56}Fe = +0.02 \pm 0.03$, Weyer and Ionov, 2007; Dauphas et al., 2009a).

4.2. Iron isotopic compositions of OIBs and related samples

Relative to MORBs, 47 OIBs display a slightly larger variation in Fe isotopic composition (Fig. 4), with δ^{56}Fe values ranging from +0.09 to +0.18‰ in 23 samples from the Society Islands and Cook-Austral chain, from +0.05 to +0.14‰ in 20 samples from Koolau, Hawaii and +0.05 to +0.09‰ in four samples from Loihi, Hawaii. These values agree well with the high-precision OIB δ^{56}Fe data available ($n = 12$; Weyer and Ionov, 2007; Teng et al., 2008; Schuessler et al., 2009; Craddock and Dauphas, 2010).

5. DISCUSSION

Large linearly correlated Mg and Fe isotopic variations are found in Hawaiian olivines resulting from kinetic isotope fractionation during inter-diffusion of Mg and Fe, with olivines isotopically either heavier or lighter than basaltic melts depending on the directions of interdiffusion (Teng et al., 2011). Hence, the isotopic difference between olivines and basaltic melts cannot be used to estimate equilibrium fractionation factors. When compared to olivine

Author's personal copy

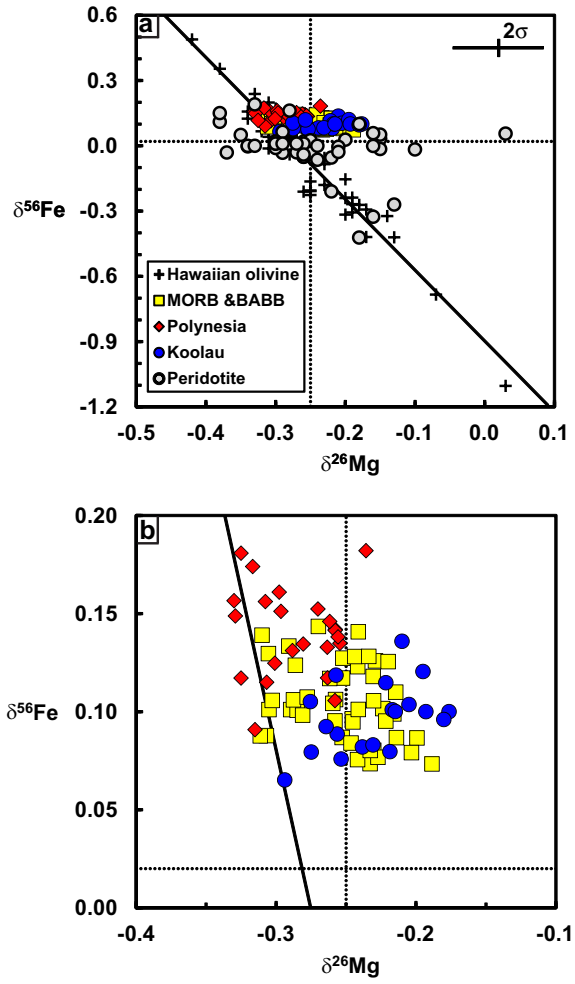

Fig. 5. $\delta^{56}Fe$ vs. $\delta^{26}Mg$ in oceanic basalts and peridotite xenoliths. $\delta^{56}Fe$ data of oceanic basalts are reported in Tables 1 and 2. $\delta^{26}Mg$ data are from Teng et al. (2010). $\delta^{56}Fe$ data of peridotites are from Weyer and Ionov (2007) and Huang et al. (2011c). $\delta^{26}Mg$ data of peridotites are from Pogge von Strandmann et al. (2011). The solid line in both panels ($\delta^{56}Fe = -3.258 \times \delta^{26}Mg - 0.897$) represents the Mg and Fe isotope fractionation line in olivine fragments from Hawaiian basalts (Teng et al., 2011). The dashed lines in both panels represent the average Mg and Fe isotopic compositions of the mantle (Weyer and Ionov, 2007; Dauphas et al., 2009a, 2010; Teng et al., 2010). Panel b only displays MORB, BABB, Koolau, French Polynesia (Society Islands and Cook-Austral chain) data.

fragments from Hawaiian basalts, basaltic samples have much narrower ranges in Mg and especially Fe isotopic compositions (Fig. 5). This difference reflects mass balance effects. While individual crystals can present large isotopic fractionation due to diffusive processes, the bulk of the crystals have compositions that are close to that of the melt, which limits the magnitude of the isotope fractionation that can be created in the liquid. When compared to Mg isotopes, Fe isotopes display larger variation in whole rocks and in minerals (Fig. 5). This is quantitatively explained by theoretical simulations that predict variations in $\delta^{56}Fe$ that are about three times greater than that in $\delta^{26}Mg$ during inter-diffusion of Mg–Fe between olivine and melt (Dauphas et al., 2010). In simple terms, the fluxes of Mg and Fe are equal in magnitude and opposite in direction in olivine. Olivine has more Mg than Fe, so diffusing Mg atoms are mixed with a larger amount of background atoms with normal isotopic composition than is the case for Fe.

In contrast to the homogenous Mg isotopic composition of oceanic basalts (Teng et al., 2010), Fe isotopic variation in oceanic basalts is significant (Fig. 5). Iron isotopic compositions of basalts can potentially be affected by seafloor alteration (Rouxel et al., 2003; Williams et al., 2009), source heterogeneity, degree of partial melting (Williams et al., 2004, 2005, 2009; Weyer et al., 2005; Weyer and Ionov,

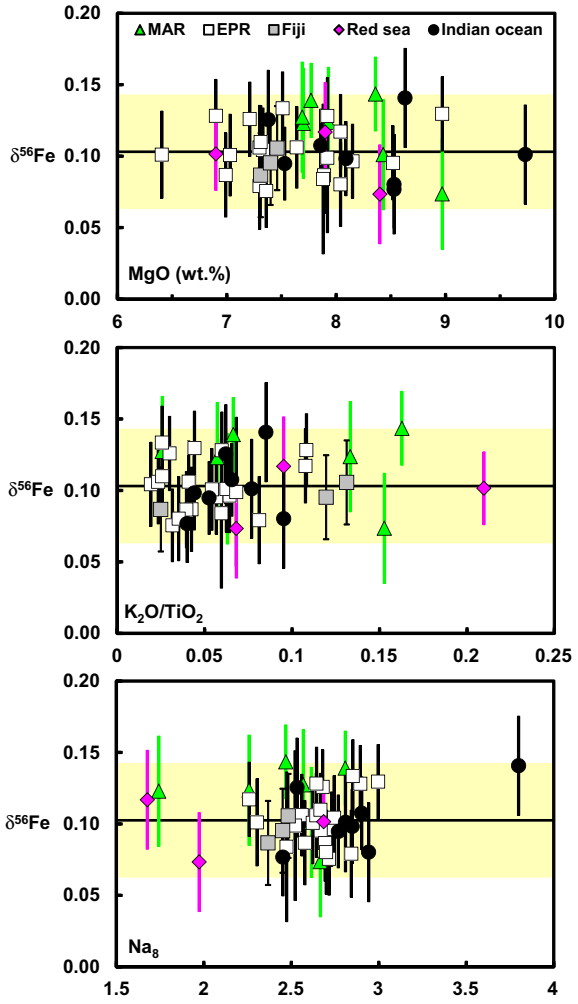

Fig. 6. $\delta^{56}Fe$ vs. MgO, K_2O/TiO_2 and Na_8 in MORBs and BABBs investigated in this study. The highly to moderately incompatible element ratio of K_2O/TiO_2 has been used to classify different types of MORBs (Reynolds et al., 1992). $Na_8 = Na_2O + 0.373 \times MgO - 2.98$ (Klein and Langmuir, 1987), which is used to correct for the effects of fractionation in the shallow magma chamber. Lower Na_8 indicates higher degrees of partial melting and vice versa (Klein and Langmuir, 1987). Grey bar and horizontal solid line represent average $\delta^{56}Fe$ and two standard deviation of the average $\delta^{56}Fe$ of all MORBs, respectively. Data are from Table 1.

Author's personal copy

2007; Dauphas et al., 2009a; Zhao et al., 2010, 2012; Huang et al., 2011c; Hibbert et al., 2012) and post-melting processes during rise of deep-seated basaltic melts, such as fractional crystallization (Teng et al., 2008, 2011; Schuessler et al., 2009; Weyer and Seitz, 2012) and wall-rock assimilation (Schoenberg and von Blanckenburg, 2006). Basalt samples studied here are unaltered, as evidenced by previous studies of volatile and radiogenic isotopes (Devey et al., 1990; Chauvel et al., 1992; Woodhead et al., 1993; Marty and Humbert, 1997; Lassiter and Hauri, 1998; Marty and Tolstikhin, 1998; Marty and Zimmermann, 1999; Marty and Dauphas, 2003). Influence of seafloor alteration on Fe isotope measurements can be ruled out.

5.1. Iron isotopic systematics of MORBs

All MORB samples have similar Fe isotopic composition, even though they are widely dispersed and chemically diverse. Statistical tests also confirm this; the calculated reduced χ^2 (or MSWD, Mean Square Weighted Deviation) value is 1.9 and the 95% confidence interval for $n-1=42$ degrees of freedom is $0.6 <$ reduced $\chi^2 < 1.5$, if the dispersion in the measured values is well explained by the uncertainties of the individual data points. The reduced χ^2 falls out of the expected range but is very small, which suggests that most of these MORBs sample a homogenous Fe isotopic reservoir. In addition, δ^{56}Fe does not vary with indicators of magmatic differentiation (MgO), source enrichment (K_2O/TiO_2) or with degree of partial melting (Na_8) (Fig. 6). For the observed ranges in MgO content (6.5–9.8%) and Na_8 (1.7–3.8), the expected fractionation in Fe isotopes is limited, which explains the constant δ^{56}Fe value of MORBs.

MORBs are consistently heavier ($\delta^{56}Fe = +0.105‰$) than their mantle source ($\delta^{56}Fe = \sim+0.02 \pm 0.03‰$, Weyer and Ionov, 2007) (Fig. 4), which mainly reflects Fe isotope fractionation during partial melting of the mantle. Theoretical studies suggest that the degree of Fe isotope fractionation during partial melting depends on the degree of partial melting (F), the $Fe^{3+}/\Sigma Fe$ of the source and the type of melting (buffered vs. non-buffered) (Dauphas et al., 2009a). Isotope fractionation is expected to decrease with F and increase with $Fe^{3+}/\Sigma Fe$ of the source. The range in the degree of partial melting during the production of MORBs varies from 6% to 20% (Klein and Langmuir, 1987; Workman and Hart 2005), which alone will produce no more than 0.02‰ δ^{56}Fe isotopic variation (Dauphas et al., 2009a). Although the estimated average $Fe^{3+}/\Sigma Fe$ ratios of MORBs vary from 0.07 ± 0.03 (2σ) (Christie et al., 1986), 0.12 ± 0.04 (2σ) (Bezos and Humler, 2005) to 0.16 ± 0.02 (2σ) (Cottrell and Kelley, 2011), all these studies show that the $Fe^{3+}/\Sigma Fe$ ratios of MORBs vary little. As shown in Dauphas et al. (2009a), a ~0.3‰ fractionation between Fe^{2+} and Fe^{3+} and a melt $Fe^{3+}/\Sigma Fe$ ratio of 0.16 at 10% partial melting can produce ~0.04‰ Fe isotope fractionation between MORBs and their mantle source. This is insufficient to explain the MORB data but further isotopic fractionation may be present between Fe^{2+} in melt and mantle minerals. Clearly, work has to be done to estimate equilibrium Fe isotope fractionation in phases and P–T conditions relevant to mantle melting.

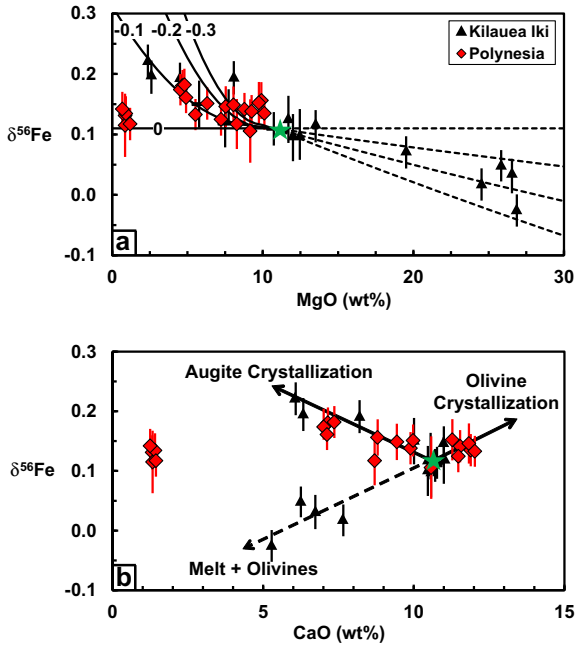

Fig. 7. a) δ^{56}Fe vs. MgO and b) δ^{56}Fe vs. CaO for OIBs from the Society Islands and Cook-Austral chain, French Polynesia. Data are reported in Table 2. MgO and CaO data (Helz et al., 1994) and δ^{56}Fe data (Teng et al., 2008) of Kilauea Iki lavas are also plotted for comparison. (a) Solid lines represent calculated Fe isotopic compositions of residual melts during fractional crystallization of olivines by assuming a Rayleigh distillation process with average crystal-melt fractionation factors ($\Delta\delta^{56}Fe_{crystal-melt} = \delta^{56}Fe_{crystal} - \delta_{56}Fe_{melt}$) of 0, −0.1‰, −0.2‰ and −0.3‰. Dashed lines represent calculated mixing lines between the most magnesian melt from the 1959 eruption (green star, MgO = 10.7 wt.% and $\delta^{56}Fe = +0.11‰$) and the most magnesian olivines ($MgO = 46.6 \pm 1$ wt.% and $\delta^{56}Fe = +0.11‰$, 0‰, −0.1‰ and −0.2‰). See Teng et al. (2008) for details on the modelling. (b) Solid lines represent expected Fe isotopic compositions of residual melts during fractional crystallization of olivines (olivine-bearing samples) or augite (olivine-free differentiates) for Kilauea Iki lavas.

5.2. Iron isotopic systematics of OIBs

When compared to the mantle ($\delta^{56}Fe = +0.02 \pm 0.03‰$, Weyer and Ionov, 2007), the average Fe isotopic composition of OIBs is also heavy ($\delta^{56}Fe = +0.1‰$) to an extent comparable to that of MORBs (Fig. 4). This mantle-melt difference mainly reflects Fe isotope fractionation during partial melting. However, in contrast to MORBs, the Fe isotopic compositions of OIBs are heterogeneous (Fig. 4) and may reflect processes other than partial melting such as fractional crystallization and source heterogeneity. As shown in previous studies, fractional crystallization of OIBs can significantly fractionate Fe isotopes, with olivine cumulates evolving towards lighter isotopic compositions and remaining melts evolving towards heavier isotopic compositions (Teng et al., 2008, 2011; Schuessler et al., 2009; Weyer and Seitz, 2012). Below, we discuss Fe isotopic systematics of the Society Islands and Cook-Austral chain, and Koolau in turn.

Author's personal copy

5.2.1. Iron isotopic systematics of the Society Islands and Cook-Austral chain

Basalt samples with 4 wt.% < MgO < 11 wt.% from the Society Islands and Cook-Austral chain have relatively heavy Fe isotopic compositions compared to MORBs and fall on the fractional crystallization lines defined by Kilauea Iki lavas (Fig. 7a). Petrographic and geochemical studies show that olivine and clinopyroxene are the major fractioning phases in these samples (Devey et al., 1990). Previous studies suggested that olivine and clinopyroxene tended to have light Fe isotopic composition relative to melts (Teng et al., 2008, 2011; Dauphas et al., 2009a). The heavy Fe isotopic compositions of some basalts from the Society Islands and Cook-Austral chain may reflect the removal of different amount of isotopically light olivine and clinopyroxene. The Fe isotopic variations in these samples can be modeled by Rayleigh fractionation with average crystal-melt fractionation factors (Δ^{56}Fe) of ~−0.1‰ to −0.3‰, similar to Kilauea Iki lavas (Teng et al., 2008).

Further support for this interpretation comes from the relationship between δ^{56}Fe and CaO in these samples. Although fractional crystallization of olivine and clinopyroxene produces isotopically heavy melt, it is difficult to distinguish the role of these two minerals in controlling the Fe isotopic composition of the melt on a δ^{56}Fe vs. MgO plot (e.g., Fig. 7a). This is because crystallization of olivine and clinopyroxene both results in a decrease in MgO content and increase in δ^{56}Fe in the melts (Helz, 1987; Helz et al., 1994). Hence, samples produced by fractional crystallization of these two minerals are expected to follow similar trends on the δ^{56}Fe vs. MgO plot (Fig. 7a). By contrast, crystallization of olivine vs. clinopyroxene is easy to tell on a δ^{56}Fe vs. CaO plot (Fig. 7b) because removal of olivine results in an increase in CaO content whereas removal of clinopyroxene results in a decrease in CaO content in the melt. Removal of plagioclase can also lead to a decrease in CaO content in the residual melt but this should not affect the melt Fe isotopic composition due to its much lower FeO content than that of the residual melt. Samples produced by crystallization of olivine are therefore expected to have a positive correlation between δ^{56}Fe vs. CaO whereas those produced by removal of clinopyroxene are expected to display a negative correlation. Olivine-bearing samples and olivine-free internal differentiates from Kilauea Iki lava lake define both olivine and clinopyroxene crystallization trends (Fig. 7b). Samples from the Society Islands and Cook-Austral chain fall on both trends (Fig. 7b), suggesting their isotopically heavy Fe isotopic compositions are produced by crystallization of both minerals.

The low-MgO samples (MgO = 0.68 to 1.19 wt.%) from the Society Islands have MORB-like Fe isotopic compositions and are more differentiated than any of the Kilauea Iki samples, which may reflect distinct behaviors of Fe isotopes during crystallization of different minerals. All these samples fall on a crystallization line with the average crystal-melt fractionation factor of 0 (Fig. 7a). These evolved samples are thought to be derived by the removal of up to 70% cumulates from basalts, which include olivine, plagioclase, pyroxene and other Fe-bearing minerals (Devey et al., 1990; Hekinian et al., 1991). In contrast to olivine and pyroxene, plagioclase and Fe-bearing minerals like ilmenite and magnetite have heavy Fe isotopic composition relative to melts (Polyakov et al., 2007; Heimann et al., 2008; Shahar et al., 2008; Millet and Baker, 2009; Craddock et al., 2010; Dauphas et al., 2012). Fractional crystallization of isotopically heavy Fe-bearing oxide minerals during late-stage differentiation might offset the effects of early-stage olivine and clinopyroxene crystallization and bring back the residual melts near the starting MORB-like isotopic composition, especially considering the relatively low Fe content of these residual melts (FeO = 4.23–4.77 wt.%). This might explain why the low-MgO samples from the Society Islands display limited Fe isotope fractionation relative to MORBs. Nonetheless, other processes like source heterogeneity and different melting processes on these samples cannot be excluded.

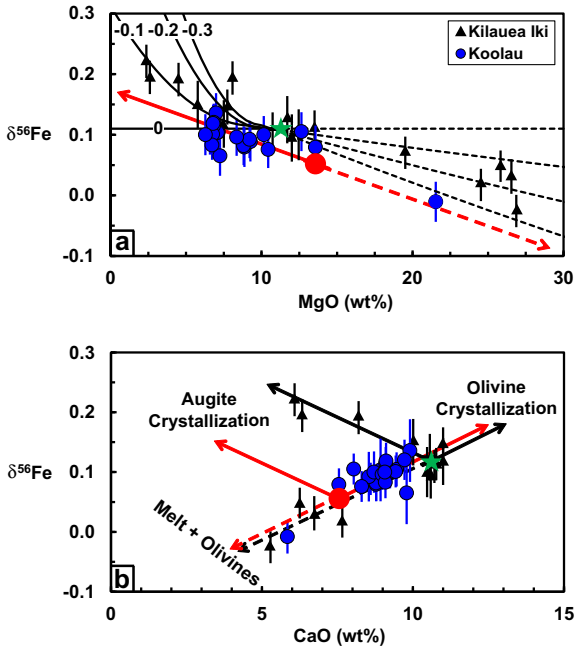

Fig. 8. (a) δ^{56}Fe vs. MgO and (b) δ^{56}Fe vs. CaO for OIBs from Koolau, Hawaii. Data are from Table 2. Data and modelling of Kilauea Iki lavas from Teng et al. (2008) are also plotted in both panels for comparison (CaO data for Kilauea Iki lavas are from Helz et al., 1994). The red dots represent the potential parental magma of Koolau lavas (MgO = 13.57 wt.%, CaO = 7.55 wt.% and δ^{56}Fe = +0.06‰). The red solid and dashed lines represent fractional crystallization and mixing lines for Koolau samples, respectively. See text for details. (For interpretation of the references to colour in this figure legend, the reader is referred to the web version of this article.)

5.2.2. Iron isotopic systematics of Koolau, Hawaii

Olivine is the dominant phenocryst phase in the Koolau samples (Frey et al., 1994). Iron isotopic variations in Koolau samples, similar to Kilauea Iki lavas, can also be explained by fractional crystallization of isotopically light olivines. Analysis of olivine fragments from an olivine cumulate sample in Koolau volcano (KOO17A) confirms this. These olivine fragments display large Fe isotopic variation, with δ^{56}Fe ranging from light (−0.04‰) to heavy

Author's personal copy

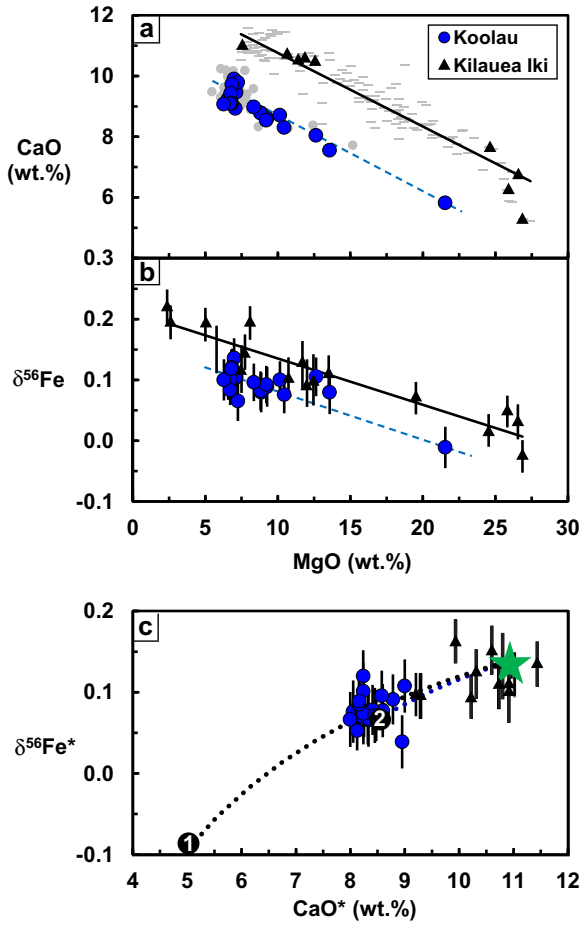

Fig. 9. (a) CaO vs. MgO, (b) δ^{56}Fe vs. MgO and (c) olivine-fractionation-adjusted δ^{56}Fe ($\delta^{56}Fe^*$) vs. olivine-fractionated-adjusted CaO (CaO^*) for OIBs from Koolau, Hawaii. Grey bars represent all samples from Kilauea Iki lava lake (Helz et al., 1994) and grey solid circles represent all samples analyzed for Koolau samples in Frey et al. (1994). In (a) solid line represents the best fitting line for all Kilauea Iki lavas with MgO > 7.5 wt.%. Kilauea Iki lavas with MgO < 7.5 wt.% are affected by crystallization of clinopyroxene (augite) and plagioclase and hence are excluded. Dashed line represents the best fitting line for Koolau samples. In panel (b) solid line represents the best fitting line for all Kilauea Iki lavas analyzed for Fe isotopes (Teng et al., 2008). Dashed line represents the best fitting line for Koolau samples. $\delta^{56}Fe^*$ and CaO^* in (c) are Fe isotopic composition and CaO contents of basalts that are adjusted for olivine crystallization by using correlations between CaO vs. MgO, and δ^{56}Fe vs. MgO in samples from Kilauea Iki lavas (a and b) to MgO = 10.7 wt.%. The two dotted lines represent mixing lines between the picrite end member, represented by Kilauea samples as a green star ($FeO^* = 10.95$ wt.%, $CaO^* = 11$ wt.%, $\delta^{56}Fe^* = +0.14‰$), and (1) dacite model ($FeO^* = 5.18$ wt.%, $CaO^* = 4.93$ wt.%, $\delta^{56}Fe^* = -0.1‰$), and (2) pyroxenite model ($FeO^* = 8.13$ wt.%, $CaO^* = 8.58$ wt.%, $\delta^{56}Fe^* = +0.07‰$). See text for details and references.

values (+0.18‰) (Teng et al., 2011). The whole-rock olivine cumulate sample (KOO17A) also has light Fe isotopic composition ($\delta^{56}Fe = -0.01‰$), close to the light end of olivine fragments (Fig. 8). By using the sample KM-1 with the highest MgO (13.57 wt.%) and lowest CaO (7.55 wt.%) content among all Koolau samples (except the cumulate sample KOO17A) and a δ^{56}Fe value of +0.06‰ to represent the starting melt, all Koolau samples can be explained by fractional crystallization of isotopically light olivines (Fig. 8b).

Although olivine crystallization can explain both Kilauea Iki and Koolau samples, Koolau samples have lower CaO content and δ^{56}Fe value than Kilauea Iki ones at the same MgO content (Fig. 9a and b). The olivine-fractionation-adjusted ($\delta^{56}Fe^*$) values correlate positively with the olivine-fractionation-adjusted (CaO^*) contents, with the Koolau samples slightly heavier than Kilauea Iki lavas (Fig. 9c). This slight Fe isotopic difference between Koolau and Kilauea Iki lavas may reflect different conditions during partial melting e.g., different degrees of partial melting or oxidation fugacity, or source heterogeneity. Previous studies have found linear correlations between MnO content and olivine-adjusted contents of SiO_2 and MgO contents as well as Nd–Hf–Pb isotopic compositions and La/Nb ratio in Koolau lavas (Huang and Frey, 2005; Huang et al., 2007). These correlations have been interpreted to reflect two-end member mixing. One end-member is a picritic melt that is generated by garnet peridotite melting, as represented by Kilauea lavas. The other end member is a dacite melt produced by small degree (10–20%) partial melting of eclogites, derived from recycled oceanic crust (e.g., Hauri, 1996; Huang et al., 2007) or a high-SiO_2, high-MgO melt derived from ~40% degree of partial melting of secondary garnet pyroxenite that is produced by reactions of peridotite with SiO_2-rich melt formed from partial melting of eclogite (Sobolev et al., 2005, 2007). These two silicate-rich melt end-members have been tested by using Fe/Mn ratio and major elemental data of Koolau and Kilauea samples (Huang et al., 2007). The dacite model (Hauri, 1996; Huang et al., 2007) seems to explain the Fe/Mn–SiO_2 correlation better than the pyroxenite model (Sobolev et al., 2005, 2007). Iron isotopic data of Koolau and Kilauea lavas may help to further evaluate these two models. Both models can fit the correlation between the olivine-fractionation-adjusted δ^{56}Fe ($\delta^{56}Fe^*$) and olivine-fractionation-adjusted CaO (CaO^*) contents (Fig. 9c) but the dacite model requires that the dacite melt end-member produced from eclogite has a $\delta^{56}Fe^*$ value of ~−0.1‰ whereas the secondary pyroxenite model requires that the SiO_2-rich melt end-member derived from secondary garnet pyroxenite has a $\delta^{56}Fe^*$ value of ~+0.07‰. Although these end-member $\delta^{56}Fe^*$ values are not unique, the main point that these two different models require distinct $\delta^{56}Fe^*$ value is robust. Therefore, the behaviors of Fe isotopes during partial melting of eclogites can provide some clues on these two models. To date, no studies have been done on Fe isotope fractionation during partial melting of eclogites. Nonetheless, studies of eclogites reveal ~0.6‰ Fe isotopic variation, with δ^{56}Fe values ranging from values of −0.4‰ to +0.2‰, and ~0.3‰ inter-mineral Fe isotope fractionation, with garnet ($\delta^{56}Fe = -0.27$ to +0.40‰) consistently lighter than coexisting omphacite ($\delta^{56}Fe = -0.14$ to +0.38‰) (Williams et al., 2009). Although melts from eclogites are expected to have heavier Fe isotopic composition than residue, the large Fe isotopic variations in eclogites and in eclogite minerals make it difficult to rule out any of these two models. None-

Author's personal copy

theless, Fe isotopes could be a potential tracer for variations in source lithology.

5.3. Implications for the Fe isotopic composition of the Earth and other planets

The Fe isotopic composition of the Earth can place important constraints on the differentiation and evolution of the inner solar system (e.g., Poitrasson et al., 2004; Dauphas and Rouxel, 2006). However, it is still debated whether the Earth has a chondritic Fe isotopic composition or not (Williams et al., 2004, 2005; Weyer et al., 2005, 2007; Schoenberg and von Blanckenburg, 2006; Beard and Johnson, 2007; Poitrasson, 2007; Weyer and Ionov, 2007; Dauphas et al., 2009a, 2010; Zhao et al., 2010, 2012; Huang et al., 2011c). MORBs, OIBs and continental basalts have on average, heavier Fe isotopic compositions than chondrites, which has been interpreted as the Earth has a supra-chondritic Fe isotopic composition. By contrast, studies of mantle xenoliths (Williams et al., 2004, 2005; Weyer et al., 2005; Schoenberg and von Blanckenburg, 2006; Weyer and Ionov 2007; Zhao et al., 2010, 2012; Huang et al., 2011c) and subduction-related magmas (e.g., some island arc basalts and boninites) or komatiites produced by large degree of partial melting (Dauphas et al., 2009a, 2010; Hibbert et al., 2012) indicate that the Earth may have identical Fe isotopic composition to the chondrites while the isotopically heavy basalts might result from Fe isotope fractionation during partial melting of the upper mantle and differentiation of basaltic magmas.

Examination of >90 oceanic basalts here confirms previous studies that basalts are isotopically heavier than chondrites and mantle xenoliths (Beard et al., 2003; Poitrasson et al., 2004; Weyer et al., 2005; Weyer and Ionov, 2007), but it is the first study to systematically measure oceanic basalts at high precision (~±0.03‰). It reveals a small, but measureable Fe isotopic variation between MORBs and OIBs. These differences among MORBs, OIBs and mantle xenoliths are best explained by mantle heterogeneity and Fe isotope fractionation during partial melting and subsequent fractional crystallization of basaltic magma in OIBs. Differentiated igneous rocks like basalts should not be used to estimate the Fe isotopic compositions of their source mantles. Mantle xenoliths more likely preserve mantle Fe isotopic signatures and can provide better estimates of the Fe isotopic composition of the mantle once the effects of partial melting and metasomatism are carefully assessed (e.g., Williams et al., 2004, 2005; Weyer et al., 2005; Weyer and Ionov 2007; Zhao et al., 2010, 2012; Huang et al., 2011c). Although it is uncertain whether Fe isotope fractionation during partial melting and fractional crystallization occurs in other planetary bodies or not (Poitrasson et al., 2004; Weyer et al., 2005, 2007; Schoenberg and von Blanckenburg, 2006; Beard and Johnson, 2007; Poitrasson, 2007; Weyer and Ionov, 2007; Dauphas et al., 2009a; Liu et al., 2010; Williams et al., 2012), studies aimed at comparing the Fe isotopic composition of differentiated planetary bodies in the solar system need to take into account the possibility of Fe isotope fractionation during igneous processes. For instance, a recent study has shown that angrites have Fe isotopic compositions that are very close to MORBs and are fractionated relative to chondrites (Wang et al., 2012).

6. CONCLUSIONS

The main conclusions to be drawn from our high-precision Fe isotopic analyses of MORBs, OIBs and BABBs are:

(1) MORBs (mostly quenched submarine glasses) display a limited Fe isotopic variation with δ^{56}Fe ranging from +0.07‰ to +0.14‰ and an average $\delta^{56}Fe = +0.105 \pm 0.006‰$ ($2SD/\sqrt{n}$, $n = 43$). The homogenous Fe isotopic composition reflects limited variation in the degree of partial melting and fractional crystallization of the MORBs investigated here, as evidenced by their limited range in MgO.
(2) Three BABBs from the North Fiji basin have δ^{56}Fe ranging from +0.09‰ to +0.11‰, similar to MORBs.
(3) OIBs have heterogeneous Fe isotopic compositions, with δ^{56}Fe ranging from +0.05‰ to +0.14‰ in Koolau, Hawaii, from +0.05‰ to +0.09‰ in Loihi, Hawaii and from +0.09‰ to +0.18‰ in the Society Islands and Cook-Austral chain. The isotopic heterogeneity in OIBs mainly reflects fractional crystallization of olivine and pyroxene, in addition to source heterogeneity.
(4) The average Fe isotopic compositions of MORBs, OIBs and BABBs are heavier than mantle peridotites. This difference reflects Fe isotope fractionation during partial melting possibly modulated by redox conditions.
(5) Iron isotopic composition of basalts should not be used to directly estimate that of their source unless the degree of isotope fractionation during their petrogenesis is quantified.

ACKNOWLEDGEMENTS

We thank Haolan Tang for help in the clean lab, Karsten Hansse for unpublished major element data for two OIB samples, Roz Helz and Frank Richter for discussions. The constructive comments from Helen Williams, Jasper Konter, Sune Nielsen and Bill White, and careful and efficient editing from Janne Blichert-Toft are greatly appreciated. This work was supported by NSF (EAR-0838227 and EAR-1056713) and Arkansas Space Grant Consortium (SW19002) to Fang-Zhen Teng; NSF (EAR-0820807), NASA (NNX09AG59G, NNX12AH60G) and a Packard fellowship to Nicolas Dauphas; and NSF (EAR-1144727) to Shichun Huang.

REFERENCES

Beard B. L. and Johnson C. M. (2007) Comment on "Iron isotope fractionation during planetary differentiation" by S. Weyer

Author's personal copy

et al., Earth Planet. Sci. Lett. V240, pp. 251–264. *Earth Planet. Sci. Lett.* **256**(3–4), 633–637.

Beard B. L., Johnson C. M., Skulan J. L., Nealson K. H., Cox L. and Sun H. (2003) Application of Fe isotopes to tracing the geochemical and biological cycling of Fe. *Chem. Geol.* **195**(1–4), 87–117.

Bezos A. and Humler E. (2005) The $Fe^{3+}/\Sigma Fe$ ratios of MORB glasses and their implications for mantle melting. *Geochim. Cosmochim. Acta* **69**(3), 711–725.

Bigeleisen J. and Mayer M. G. (1947) Calculation of equilibrium constants for isotopic exchange reactions. *J. Chem. Phys.* **15**(5), 261–267.

BVSP (1981) *Basaltic Volcanism on the Terrestrial Planets*. Pergamon, New York, 1286 pp.

Chauvel C., Hofmann A. W. and Vidal P. (1992) HIMU-EM: the French Polynesian connection. *Earth Planet. Sci. Lett.* **110**, 99–119.

Chauvel C., Maury R. C., Blais S., Lewin E., Guillou H., Guille G., Rossi P. and Gutscher M.-A. (2012) The size of plume heterogeneities constrained by Marquesas isotopic stripes. *Geochem. Geophys. Geosyst.* **13**, Q07005. http://dx.doi.org/10.1029/2012GC004123.

Christie D. M., Carmichael I. S. E. and Langmuir C. H. (1986) Oxidation states of mid-ocean ridge basalt glasses. *Earth Planet. Sci. Lett.* **79**(3–4), 397–411.

Cottrell E. and Kelley K. A. (2011) The oxidation state of Fe in MORB glasses and the oxygen fugacity of the upper mantle. *Earth Planet. Sci. Lett.* **305**, 270–282.

Craddock P. R. and Dauphas N. (2010) Iron isotopic compositions of reference materials, geostandards and chondrites. *Geostand. Geoanal. Res.* **35**, 101–123.

Craddock P. R., Dauphas N. and Clayton R. N. (2010) Mineralogical control on iron isotopic fractionation during lunar differentiation and magmatism. *LPSC*, 41, #1230.

Craddock P. R., Warren J. M., Dauphas N. (2013) Abyssal peridotites reveal the near-chondritic Fe isotopic composition of the Earth. *Earth Planet. Sci. Lett.* http://dx.doi.org/10.1016/j.epsl.2013.01.011.

Dauphas N. and Marty B. (1999) Heavy nitrogen in carbonatites of the Kola penninsula: a possible signature of the deep mantle. *Science* **286**, 2488–2490.

Dauphas N., van Zuilen M., Wadhwa M., Davis A. M., Marty B. and Janney P. E. (2004) Clues from Fe isotope variations on the origin of early Archean BIFs from Greenland. *Science* **306**(5704), 2077–2080.

Dauphas N., Craddock P. R., Asimow P. D., Bennett V. C., Nutman A. P. and Ohnenstetter D. (2009a) Iron isotopes may reveal the redox conditions of mantle melting from Archean to Present. *Earth Planet. Sci. Lett.* **288**(1–2), 255–267.

Dauphas N., Pourmand A. and Teng F.-Z. (2009b) Routine isotopic analysis of iron by HR-MC-ICPMS: how precise and how accurate? *Chem. Geol.* **267**, 175–184.

Dauphas N. and Rouxel O. (2006) Mass spectrometry and natural variations of iron isotopes. *Mass Spectrom. Rev.* **25**, 515–550.

Dauphas N., Teng F.-Z. and Arndt N. T. (2010) Magnesium and iron isotopes in 2.7 Ga Alexo komatiites: mantle signatures, no evidence for Soret diffusion, and identification of diffusive transport in zoned olivine. *Geochim. Cosmochim. Acta* **74**, 3274–3291.

Dauphas N., Roskosz M., Alp E. E., Golden D. C., Sio C. K., Tissot F. L. H., Hu M. Y., Zhao J., Gao L. and Morris R. V. (2012) A general moment NRIXS approach to the determination of equilibrium Fe isotopic fractionation factors: application to goethite and jarosite. *Geochim. Cosmochim. Acta* **94**, 254–275.

Devey C., Albarede F., Cheminee J. L., Michard A., Muhe R. and Stoffers P. (1990) Active submarine volcanism on the Society hot spot swell: a geochemical study. *J. Geophys. Res.* **95**, 5049–5070.

Eiler J. M., Farley K. A., Valley J. W., Hauri E., Craig H., Hart S. R. and Stolper E. M. (1997) Oxygen isotope variations in ocean island basalt phenocrysts. *Geochim. Cosmochim. Acta* **61**, 2281–2293.

Frey F. A., Garcia M. O. and Roden M. F. (1994) Geochemical characteristics of Koolau Volcano: implications of intershield geochemical differences among Hawaiian volcanoes. *Geochim. Cosmochim. Acta* **58**, 1441–1462.

Hart S. R., Hauri E. H., Oschmann L. A. and Whitehead J. A. (1992) Mantle plumes and entrainment: isotopic evidence. *Science* **256**, 517–520.

Hauri E. H. (1996) Major-element variability in the Hawaiian mantle plume. *Nature* **382**, 415–419.

Heimann A., Beard B. L. and Johnson C. M. (2008) The role of volatile exsolution and sub-solidus fluid/rock interactions in producing high $^{56}Fe/^{54}Fe$ ratios in siliceous igneous rocks. *Geochim. Cosmochim. Acta* **72**(12), A362–A363.

Hekinian R., Bideau D., Stoffers P., Cheminee J. L., Muhe R., Puteanus D. and Binard N. (1991) Submarine intraplate volcanism in the South Pacific: geological setting and petrology of the Society and the Austral regions. *J. Geophys. Res.* **96**(B2), 2109–2138.

Helz R. T. (1987) Differentiation behavior of Kilauea Iki lava lake, Kilauea Volcano, Hawaii: an overview of past and current work. In *Magmatic Processes: Physiochemical Principles*, vol. 1 (ed. B. O. Mysen). Geochem. Soc. Spec. Publ., pp. 241–258.

Helz R. T., Kirschenbaum H., Marinenko J. W. and Qian R. (1994) Whole rock analyses of core samples from the 1967, 1975, 1979 and 1981 drillings of Kilauea Iki lava lake, Hawaii. *US Geol. Survey Open File Report*, 94–684.

Hibbert K. E. J., Williams H. M., Kerr A. C. and Puchtel I. S. (2012) Iron isotopes in ancient and modern komatiites: evidence in support of an oxidised mantle from Archean to present. *Earth Planet. Sci. Lett.* **321–322**, 198–207.

Hofmann A. W. (2003) Sampling mantle heterogeneity through oceanic basalts: isotopes and trace elements. In *The Mantle and Core. Treatise on Geochemistry* (ed. R. W. Carlson). Elsevier-Pergamon, Oxford, pp. 61–101.

Huang S. and Frey F. A. (2005) Recycled oceanic crust in the Hawaiian Plume: evidence from temporal geochemical variations within the Koolau Shield. *Contrib. Miner. Petrol.* **149**(5), 556–575. http://dx.doi.org/10.1007/s00410-005-0664-9.

Huang S., Humayun M. and Frey F. A. (2007) Iron/manganese ratio and manganese content in shield lavas from Ko'olau Volcano, Hawai'i. *Geochem. Cosmochim. Acta* **71**, 4557–4569.

Huang S., Farkas J. and Jacobsen S. B. (2011a) Stable calcium isotopic compositions of Hawaiian shield lavas: evidence for recycling of ancient marine carbonates into the mantle. *Geochem. Cosmochim. Acta* **75**, 4987–4997.

Huang S., Hall P. S. and Jackson M. G. (2011b) Geochemical zoning of volcanic chains associated with Pacific hotspots. *Nat. Geosci.* **4**, 874–878. http://dx.doi.org/10.1038/NGEO1263.

Huang F., Zhang Z., Lundstrom C. C. and Zhi X. (2011c) Iron and magnesium isotopic compositions of peridotite xenoliths from Eastern China. *Geochim. Cosmochim. Acta* **75**, 3318–3334.

Jackson M. G. and Dasgupta R. (2008) Compositions of HIMU, EM1, and EM2 from global trends between radiogenic isotopes and major elements in ocean island basalts. *Earth Planet. Sci. Lett.* **276**, 175–186.

Jackson M. G., Weis D. and Huang S. (2012) Major element variations in Hawaiian shield lavas: source features and

Author's personal copy

perspectives from global ocean island basalt (OIB) systematics. *Geochem. Geophys. Geosyst.* **13**, Q09009. http://dx.doi.org/10.1029/2012GC004268.

Klein E. and Langmuir C. H. (1987) Global correlations of ocean ridge basalt chemistry, axial depth, crustal thickness. *J. Geophys. Res.* **92**, 8080–8115.

Lassiter J. C. and Hauri E. H. (1998) Osmium-isotope variations in Hawaiian lavas: evidence for recycled oceanic lithosphere in the Hawaiian plume. *Earth Planet. Sci. Lett.* **164**(3–4), 483–496.

Liu Y., Spicuzza M. J., Craddock P. R., Day J. M. D., Valley J. W., Dauphas N. and Taylor L. A. (2010) Oxygen and iron isotope constraints on near-surface fractionation effects and the composition of lunar mare basalt source regions. *Geochim. Cosmochim. Acta* **74**(21), 6249–6262.

Marty B. and Dauphas N. (2003) The nitrogen record of crust-mantle interaction and mantle convection from Archean to present. *Earth Planet. Sci. Lett.* **206**(3–4), 397–410.

Marty B. and Humbert F. (1997) Nitrogen and argon isotopes in oceanic basalts. *Earth Planet. Sci. Lett.* **152**(1–4), 101–112.

Marty B. and Tolstikhin I. N. (1998) CO_2 fluxes from mid-ocean ridges, arcs and plumes. *Chem. Geol.* **145**(3–4), 233–248.

Marty B. and Zimmermann L. (1999) Volatiles (He, C, N, Ar) in mid-ocean ridge basalts: assessment of shallow-level fractionation and characterization of source composition. *Geochim. Cosmochim. Acta* **63**(21), 3619–3633.

McNutt M. K. and Fischer K. M. (1987) The South Pacific superswell. In *Seamounts, Islands, and Atolls* (eds. B. H. Keating, P. Fryer, R. Batiza and G. W. Boehlert). AGU Geophysical Monograph, pp. 25–34.

Millet M.-A., Baker J. A. (2009) Double-spike Fe isotope analyses of silicate minerals in volcanic rocks. *Goldschmidt Conference Abstracts*, A882.

Norman M. D. and Garcia M. O. (1999) Primitive magmas and source characteristics of the Hawaiian Plume: petrology and geochemistry of shield picrites. *Earth Planet. Sci. Lett.* **168**, 27–44.

Pogge Von Strandmann P. A. E., Elliott E., Marschall H. R., Coath C., Lai Y.-J., Jeffcoate A. B. and Ionov D. A. (2011) Variations of Li and Mg isotope ratios in bulk chondrites and mantle xenoliths. *Geochim. Cosmochim. Acta* **75**, 5247–5268.

Poitrasson F. (2007) Does planetary differentiation really fractionate iron isotopes? A comment of "Iron isotope fractionation during planetary differentiation" by S. Weyer, A. D. Anbar, G. P. Brey, C. Munker, K. Mezger and A. B. Woodland, EPSL, 240:251–264. *Earth Planet. Sci. Lett.* **256**, 484–492.

Poitrasson F. and Freydier R. (2005) Heavy iron isotope composition of granites determined by high resolution MC-ICP–MS. *Chem. Geol.* **222**(1–2), 132–147.

Poitrasson F., Halliday A. N., Lee D. C., Levasseur S. and Teutsch N. (2004) Iron isotope differences between Earth, Moon, Mars and Vesta as possible records of contrasted accretion mechanisms. *Earth Planet. Sci. Lett.* **223**(3–4), 253–266.

Poitrasson F., Levasseur S. and Teutsch N. (2005) Significance of iron isotope mineral fractionation in pallasites and iron meteorites for the core–mantle differentiation of terrestrial planets. *Earth Planet. Sci. Lett.* **234**(1–2), 151–164.

Polyakov V. B. (2009) Equilibrium iron isotope fractionation at core–mantle boundary conditions. *Science* **323**, 912–914.

Polyakov V. B., Clayton R. N., Horita J. and Mineev S. D. (2007) Equilibrium iron isotope fractionation factors of minerals: reevaluation from the data of nuclear inelastic resonant X-ray scattering and Mossbauer spectroscopy. *Geochim. Cosmochim. Acta* **71**(15), 3833–3846.

Reynolds J. R., Langmuir C. H., Bender J. F., Kastens K. A. and Ryan W. B. F. (1992) Spatial and temporal variability in the geochemistry of basalts from the East Pacific Rise. *Nature* **359**, 493–499.

Richter F. M., Dauphas N. and Teng F.-Z. (2009) Non-traditional fractionation of non-traditional isotopes: evaporation, chemical diffusion and Soret diffusion. *Chem. Geol.* **258**, 92–103.

Rouxel O., Dobbek N., Ludden J. and Fouquet Y. (2003) Iron isotope fractionation during oceanic crust alteration. *Chem. Geol.* **202**(1–2), 155–182.

Schoenberg R. and von Blanckenburg F. (2006) Modes of planetary-scale Fe isotope fractionation. *Earth Planet. Sci. Lett.* **252**(3–4), 342–359.

Schoenberg R., Marks M. A. W., Schuessler J. A., von Blanckenburg F. and Markl G. (2009) Fe isotope systematics of coexisting amphibole and pyroxene in the alkaline igneous rock suite of the Ilimaussa Complex, South Greenland. *Chem. Geol.* **258**(1–2), 65–77.

Schuessler J. A., Schoenberg R. and Sigmarsson O. (2009) Iron and lithium isotope systematics of the Hekla volcano, Iceland - Evidence for Fe isotope fractionation during magma differentiation. *Chem. Geol.* **258**(1–2), 78–91.

Shahar A., Manning C. E. and Young E. D. (2008) Equilibrium high-temperature Fe isotope fractionation between Fayalite and Magnetite: an experimental calibration. *Earth Planet. Sci. Lett.* **268**, 330–338.

Sobolev A. V., Hofmann A. W., Sobolev S. V. and Nikogosian I. K. (2005) An olivine-free mantle source of Hawaiian shield basalts. *Nature* **434**, 590–597.

Sobolev A. V., Hofmann A. W., Kuzmin D. V., Yaxley G. M., Arndt N. T., Chung S.-L., Danyushevsky L. V., Elliott E., Frey F. A., Garcia M. O., Gurenko A. A., Kamenetsky V. S., Kerr A. C., Krivolutskaya N. A., Matveienkov V. V., Nikogosian I. K., Rocholl A., Sigurdsson I. A., Sushchevskaya N. M. and Teklay M. (2007) The amount of recycled crust in sources of mantle-derived melts. *Science* **316**, 412–417.

Taylor P. D. P., Maeck R. and De Bievre P. (1992) Determination of the absolute isotopic composition and atomic weight of a reference sample of natural iron. *Int. J. Mass Spectrom.: Ion Processes* **121**, 111–125.

Telus M., Dauphas N., Moynier F., Tissot F. L. H., Teng F.-Z., Nabelek P. I., Craddock P. R. and Groat L. A. (2012) Iron, zinc, magnesium and uranium isotopic fractionation during continental crust differentiation: the tale from migmatites, granitoids, and pegmatites. *Geochim. Cosmochim. Acta* **97**, 247–265.

Teng F.-Z., Dauphas N. and Helz R. T. (2008) Iron isotope fractionation during magmatic differentiation in Kilauea Iki lava lake. *Science* **320**, 1620–1622.

Teng F.-Z., Li W.-Y., Ke S., Marty B., Dauphas N., Huang S., Wu F.-Y. and Pourmand A. (2010) Magnesium isotopic composition of the Earth and chondrites. *Geochim. Cosmochim. Acta* **74**, 4150–4166.

Teng F.-Z., Dauphas N., Helz R. T., Gao S. and Huang S. (2011) Diffusion-driven magnesium and iron isotope fractionation in Hawaiian olivine. *Earth Planet. Sci. Lett.* **308**, 317–324.

Urey H. C. (1947) The thermodynamic properties of isotopic substances. *J. Chem. Soc. (Lond.)*, 562–581.

Valbracht P. J., Staudigel H., Honda M., McDougall I. and Davies G. R. (1996) Isotopic tracing of volcanic source regions from Hawaii: decoupling of gaseous from lithophile magma components. *Earth Planet. Sci. Lett.* **144**, 185–198.

Vidal P., Chauvel C. and Brousse R. (1984) Large mantle heterogeneity beneath French Polynesia. *Nature* **307**, 536–538.

Wang K., Moynier F., Dauphas N., Barrat J.-A., Craddock P. and Sio C. K. (2012) Iron isotope fractionation in planetary crusts. *Geochim. Cosmochim. Acta* **89**, 31–45.

Author's personal copy

Weyer S. and Ionov D. A. (2007) Partial melting and melt percolation in the mantle: the message from Fe isotopes. *Earth Planet. Sci. Lett.* **259**, 119–133.

Weyer S. and Seitz H. M. (2012) Coupled lithium- and iron isotope fractionation during magmatic differentiation. *Chem. Geol.* **294–295**, 42–50.

Weyer S., Anbar A. D., Brey G. P., Munker C., Mezger K. and Woodland A. B. (2005) Iron isotope fractionation during planetary differentiation. *Earth Planet. Sci. Lett.* **240**(2), 251–264.

Weyer S., Anbar A. D., Brey G. P., Munker C., Mezger K. and Woodland A. (2007) Fe-isotope fractionation during partial melting on Earth and the current view on the Fe-isotope budges of the planets (reply to the comment of F. Poitrasson and to the comment of B. L. Beard and C. M. Johnson on "Iron isotope fractionation during planetary differentiation" by S. Weyer, A.D. Anbar, G.P. Brey, C. Munker, K. Mezger and A.B. Woodland). *Earth Planet. Sci. Lett.* **256**(638–646).

Williams H. M., McCammon C. A., Peslier A. H., Halliday A. N., Teutsch N., Levasseur S. and Burg J. P. (2004) Iron isotope fractionation and the oxygen fugacity of the mantle. *Science* **304**(5677), 1656–1659.

Williams H. M., Peslier A. H., McCammon C., Halliday A. N., Levasseur S., Teutsch N. and Burg J. P. (2005) Systematic iron isotope variations in mantle rocks and minerals: the effects of partial melting and oxygen fugacity. *Earth Planet. Sci. Lett.* **235**(1–2), 435–452.

Williams H. M., Nielsen S. G., Renac C., Griffin W. L., O'Reilly S. Y., McCammon C. A., Pearson N., Viljoen F., Alt J. C. and Halliday A. N. (2009) Fractionation of oxygen and iron isotopes by partial melting processes: implications for the interpretation of stable isotope signatures in mafic rocks. *Earth Planet. Sci. Lett.* **283**, 156–166.

Williams H. M., Wood B. J., Wade J., Frost D. J. and Tuff J. (2012) Isotopic evidence for internal oxidation of the Earth's mantle during accretion. *Earth Planet. Sci. Lett.* **321–322**, 54–63.

Woodhead J. D., Greenwood P., Harmon R. S. and Stoffers P. (1993) Oxygen isotope evidence for recycled crust in the source of EM-type ocean island basalts. *Nature* **362**, 809–813.

Workman R. K. and Hart S. R. (2005) Major and trace element composition of the depleted MORB mantle (DMM). *Earth Planet. Sci. Lett.* **231**, 53–72.

Zhao X. M., Zhang H. F., Zhu X. K., Tang S. H. and Tang Y. J. (2010) Iron isotope variations in spinel peridotite xenoliths from North China Craton: implications for mantle metasomatism. *Contrib. Miner. Petrol.* **160**(1), 1–14.

Zhao X. M., Zhang H. F., Zhu X. K., Tang S. H. and Yan B. (2012) Iron isotope evidence for multistage melt-peridotite interactions in the lithospheric mantle of eastern China. *Chem. Geol.* **292–293**, 127–139.

Zindler A. and Hart S. (1986) Chemical geodynamics. *Ann. Rev. Earth Planet. Sci.* **14**, 493–571.

Associate editor: Janne Blichert-Toft